Crystal Structure of the Low-Temperature Form and Evolution during the Phase Transition of the Electronic Properties of a Mixed-Valence Vanadium Oxide Inserting Quinuclidinium Cations

D. Riou,*,† O. Roubeau,† L. Bouhedja,‡ J. Livage,‡ and G. Férey†

Institut Lavoisier (UMR CNRS 8637), Université de Versailles−St. Quentin, 45, Avenue des Etats-Unis, 78035 Versailles, France, and Laboratoire de Chimie de la Matière Condensée (UMR CNRS 7574), Université Pierre et Marie Curie, Tour 54, 4, Place Jussieu, 75252 Paris, France

Received June 1, 1999. Revised Manuscript Received October 22, 1999

The layered solid $V^{IV}V^{V}_3O_{10}$, NC_7H_{14} is obtained either by thermal decomposition of the decavanadate $H_2V_{10}O_{28}$, $(NC_7H_{14})_4$ or by hydrothermal synthesis in the quaternary system V_2O_5:HF:quinuclidine:H_2O. It undergoes a reversible phase transition between 200 and 230 K evidenced by single-crystal X-ray diffraction, DSC, conductivity, and ESR measurements. The low-temperature two-dimensional form is orthorhombic (space group $P2_1cn$ (n*o*. 33)) with lattice parameters $a = 11.770(2)$ Å, $b = 18.289(4)$ Å, $c = 19.740(4)$ Å, $V = 4249(3)$ Å^3. The structure was solved from 4533 reflections ($I \geq 2\sigma(I)$) with reliability factors $R1(F_o) = 0.0573$ and $wR2(F_o^2) = 0.1572$. The ordering of the amines in the interlayer space is responsible for the transition and implies some changes in the geometry of the layers. The onset of a partial V^{IV}/V^{V} segregation is evidenced, which could explain the different regimes observed in the ESR and conductivity characteristics above and below the transition.

Introduction

Numerous mixed organic−inorganic vanadium oxides were recently synthesized under mild hydrothermal conditions.[1−11] These compounds can find applications as cathodic materials in lithium batteries.[3,7,8] In this large class of new compounds, the organically templated bidimensional solids present very promising possibilities. The numerous structural characterizations show only two stoichiometries for the vanadium oxides layers: $(V_3O_7)_n$ and $(V_2O_5)_n$ (n = integer). The V_3O_7 layers[3,5,9] are built up from zigzag chains of $V^{IV}O_5$ edge-sharing square pyramids connected by $V^{V}O_4$ tetrahedra. Two possibilities are encountered for the V_2O_5 composition: (i) an ordered distribution of V^{4+} and V^{5+} in square pyramidal and tetrahedral coordinations respectively;[2,4] two different types of layers are known, both constituted of isolated V_2O_8 dimers of edge-sharing square pyramids linked by VO_4 tetrahedra, (ii) a random distribution of V^{4+} and V^{5+} in square-pyramidal coordination;[6−10] the layers are built up from connected chains of edge-sharing square pyramids such as in vanadium pentoxide. TMA, V_8O_{20}[11] is unique for this stoichiometry with double layers of edge-sharing square pyramids.

We previously described[10] the structure of V_4O_{10}, NC_7H_{14}, a bidimensional vanadium oxide which inserts quinuclidinium cations in the interlayer space and undergoes a reversible solid-state transformation between 200 and 230 K. This paper deals both with the crystallographic description of the low-temperature form of V_4O_{10}, NC_7H_{14} and the evolution of the electronic properties during the transition, characterized by ESR and conductivity measurements.

Experimental Section

Synthesis. The title product was obtained from a mixture of 1 V_2O_5:1 HF:2 quinuclidine:100 H_2O (molar) according to the mild hydrothermal conditions (453 K, 24 h, autogenous pressure) given in ref 10.

X-ray Diffraction. The data collection was performed at 173 (±2) K on a Enraf-Nonius CAD-MACH3 four-circle diffractometer. The structure was solved in the acentric nonstandard space group $P2_1cn$ (no. 33) using SHELX-TL program. After location of the vanadium atoms by direct method calculations, the remaining atoms were placed using Fourier difference syntheses. The attribution of the N_i and C_{ia} ($i = 1$, 2, 3) sites was made on both topological and values of thermal motion considerations. The hydrogen atoms were found using

* Author for correspondence.
† Université de Versailles.
‡ Université Pierre et Marie Curie.

(1) Riou, D.; Férey, G. *J. Solid State Chem.* **1995**, *120*, 137−145.
(2) Riou, D.; Férey, G. *Inorg. Chem.* **1995**, *34*, 6520−6523.
(3) Nazar, L. F.; Koene, B. E.; Britten, J. F. *Chem. Mater.* **1996**, *8*, 327−329.
(4) Zhang, Y.; O'Connor, C. J.; Clearfield, A.; Haushalter, R. C. *Chem. Mater.* **1996**, *8*, 595−597.
(5) Zhang, Y.; Haushalter, R. C.; Clearfield, A. *Chem. Commun.* **1996**, 1055−1056.
(6) Zavalij, P. Y.; Whittingham, M. S.; Boylan, E. A.; Pecharsky, V. K.; Jacobson, R. A. *Z. Kristallogr.* **1996**, *211*, 464.
(7) Whittingham, M. S.; Chen, R.; Chirayil, T.; Zavalij, P. Y. *Electrochemical Society Proc.* **1996**, *96−5*, 76−85.
(8) Leroux, F.; Goward, G.; Power, W. P.; Nazar, L. F. *J. Electrochem. Soc.* **1997**, *144*, 3886−3895.
(9) Zavalij, P. Y.; Chirayil, T.; Whittingham, M. S. *Acta Crystallogr.* **1997**, *C53*, 879−880.
(10) Riou, D.; Roubeau, O.; Férey, G. *Z. Anorg. Allg. Chem.* **1998**, *624*, 1021−1025.
(11) Chirayil, T.; Zavalij, P. Y.; Whittingham, M. S. *J. Mater. Chem.* **1997**, 2193−2197.

10.1021/cm9910759 CCC: $19.00
Published on Web 12/17/1999

Table 1. Crystal Data and Structure Refinement for V_4O_{10}, NC_7H_{14}

$T = 173$ K	λ(Mo Kα) = 0.7107 Å
crystal size: 0.3 × 0.3 × 0.2 mm	
$d_{calcd} = 2.214$ g.cm^{-3}	
$\mu_l = 27.63$ cm^{-1}	
orthorhombic	space group: $P2_1cn$ (no. 33)[a]
$a = 11.770(2)$ Å	
$b = 18.289(4)$ Å	
$c = 19.740(4)$ Å	$V = 4249(2)$ Å^3, $Z = 12$
$R1(F_O) = 0.0573$, $wR2(F_O^2) = 0.1572$ for 4533 reflections $I \geq 2\sigma(I)$	
absolute structure, Flack parameter: −0.04(9)	
residual electronic density: 1.068 and −1.099 e Å^{-3}	

[a] Equivalent positions: x, y, z; $x, {}^1/_2 - y, {}^1/_2 + z$; ${}^1/_2 + x, {}^1/_2 + y, {}^1/_2 - z$; ${}^1/_2 + x, -y, -z$.

geometrical constraints. The principal crystallographic data are summarized in Table 1, and the atomic coordinates and bond lengths are listed in Tables 2 and 3, respectively.

Differential Scanning Calorimetry. DSC experiments were performed using a Perkin-Elmer DSC7 equipment within the temperature range 150−300K (heating/cooling rate 20 K min^{-1}). A double exothermic peak is observed around 225 K when temperature decreases, and an endothermic one centered at 233 K when temperature increases (Figure 1). This suggests a reversible phase transformation around 230 K.

ESR Measurements. The ESR spectra of V_4O_{10}, NC_7H_{14} powders and single crystals were recorded with a X-band Brücker spectrometer ($\nu = 9.47$ GHz) in the temperature range 4−300 K.

Conductivity Measurements. Direct-current electrical conductivity measurements were performed on single crystals. Electrical contacts were deposited at the surface of the crystal using a silver-containing epoxy resin that can be polymerized at room temperature (Epotechny). The usual four-probe geometry was used for conductivity measurements parallel to the surface of the crystal.

Discussion

Electronic Properties. The ESR spectrum of a powder exhibits a single broad line with a quasi-Lorentzian line shape centered around $g \approx 1.97$, typical of V^{4+} ions ($S = {}^1/_2$, $I = {}^7/_2$). The signal is too broad for hyperfine lines to be seen. The nonresolved hyperfine structure is probably due to interactions between paramagnetic V^{4+} ions.

A single line is also observed when ESR spectra are recorded with a single crystal. However the position g and the line width ΔH change with the orientation of the crystal in the magnetic field (Figure 2). Two extreme positions are observed for $\theta = 0°$ and $\theta = 90°$ where θ is the angle between the magnetic field H and the direction perpendicular to the layers of the crystal, suggesting that V^{4+} ions lie in an axial crystal field due to the V═O double bond. The ESR spectra can then be described by the axial Hamiltonian $H = g_{\|}\beta H_z S_z + g_{\perp}\beta(H_x S_x + H_y S_y)$ where z corresponds to the direction of the V═O double bond. The values $g_{\|} = 1.932$ and $\Delta H_{\|} = 91$ G are observed when the magnetic field is perpendicular to the layers of the crystal. They become $g_{\perp} = 1.978$ and $\Delta H_{\perp} = 64$ G when the magnetic field lies along the layers. These g values are close to those already reported for vanadium oxide. They suggest that unpaired electrons lie in the d_{xy} orbital within the axially distorted crystal field of [VO_5] square pyramids.

All ESR spectra recorded on powders or single crystal within the temperature range 4−300 K always exhibit a single line. The g values do not change significantly with temperature but the line width ΔH increases with T (Figure 3). The line shape of the ESR signal remains

Table 2. Atomic Coordinates (×10^4) and Equivalent Isotropic Displacement Parameters (Å^2 × 10^3) for V_4O_{10}, NC_7H_{14}

atoms	x	y	z	U(eq)[a]	atoms	x	y	z	U(eq)[a]
V(1)	3603(2)	7832(1)	411(1)	9(1)	O(22)	3538(12)	8572(6)	−2638(8)	50(4)
V(2)	3476(2)	7762(1)	−2895(2)	15(1)	O(23)	8567(11)	6305(7)	−2464(7)	42(4)
V(3)	3462(2)	7115(1)	−1256(1)	11(1)	O(24)	8748(11)	6322(6)	953(6)	29(3)
V(4)	8416(3)	7129(2)	−2214(2)	30(1)	O(25)	8703(10)	8607(6)	−779(6)	26(3)
V(5)	8609(2)	7775(1)	−556(1)	1(1)	O(26)	1320(9)	8710(6)	−761(5)	15(2)
V(6)	8586(2)	7156(1)	1148(1)	16(1)	O(27)	1181(10)	6317(5)	−2378(5)	19(2)
V(7)	6497(2)	7805(2)	428(1)	19(1)	O(28)	11306(11)	6410(6)	848(6)	29(3)
V(8)	6377(2)	7841(1)	−2923(1)	13(1)	O(29)	6308(10)	8682(6)	−2685(6)	21(2)
V(9)	6378(2)	7175(1)	−1232(2)	14(1)	O(30)	6460(11)	8632(7)	686(6)	30(3)
V(10)	1274(2)	7173(1)	−2191(1)	17(1)	N(1)	−28(12)	9441(6)	−1830(6)	23(3)
V(11)	1471(2)	7875(1)	−535(1)	12(1)	C(1A)	4934(17)	5457(8)	−2318(8)	31(4)
V(12)	11448(2)	7232(1)	1106(2)	17(1)	C(1B)	8915(21)	4995(12)	2270(13)	62(7)
O(1)	6761(12)	7199(7)	1166(7)	28(3)	C(1C)	321(22)	10119(8)	−1475(7)	47(5)
O(2)	5006(10)	7530(6)	−3038(5)	21(3)	C(1D)	921(23)	9310(13)	−2300(12)	74(8)
O(3)	4983(10)	7435(6)	−1317(5)	21(2)	C(1E)	10945(27)	5061(13)	2170(13)	79(10)
O(4)	1826(11)	7298(8)	−1306(6)	33(3)	C(1F)	5364(23)	5726(9)	−3005(9)	58(6)
O(5)	8200(11)	7220(7)	−1272(7)	33(3)	C(1G)	8920(18)	9426(16)	−2203(14)	100(12)
O(6)	6803(13)	7744(8)	−489(7)	36(4)	N(2)	9979(12)	5528(6)	−3469(6)	23(3)
O(7)	1807(11)	7670(7)	−2944(6)	24(3)	C(2A)	5015(17)	9542(8)	−646(9)	36(4)
O(8)	3213(10)	7277(5)	1126(6)	14(2)	C(2B)	4873(38)	9833(11)	−1841(12)	134(20)
O(9)	11668(18)	7856(6)	425(6)	53(6)	C(2C)	6211(19)	9862(13)	−697(15)	71(8)
O(10)	3165(10)	7701(7)	−486(6)	27(3)	C(2D)	4955(43)	9234(10)	−1311(11)	166(25)
O(11)	5060(10)	7570(7)	318(6)	26(3)	C(2E)	9241(19)	5763(10)	−4042(10)	47(5)
O(12)	3331(12)	7138(6)	−2226(6)	32(3)	C(2F)	4234(27)	10152(12)	−438(10)	64(8)
O(13)	8224(9)	7696(6)	362(7)	21(3)	C(2G)	1165(17)	5469(13)	−3724(14)	63(7)
O(14)	6730(13)	7257(7)	−2134(7)	32(3)	N(3)	9915(11)	5555(6)	−166(7)	23(3)
O(15)	8172(10)	7747(7)	−2973(7)	32(3)	C(3A)	4839(16)	9522(8)	−3983(8)	33(4)
O(16)	10004(10)	7507(6)	1274(6)	25(3)	C(3B)	5866(36)	9987(16)	−3860(17)	143(21)
O(17)	51(10)	7494(6)	−465(5)	23(3)	C(3C)	5307(20)	5116(9)	−212(9)	46(5)
O(18)	3519(11)	6282(6)	−1045(5)	25(3)	C(3D)	3884(41)	9989(23)	−3912(22)	191(28)
O(19)	3643(11)	8659(6)	598(5)	22(2)	C(3E)	10854(32)	5657(12)	−648(15)	109(13)
O(20)	6360(11)	6320(7)	−1008(7)	40(4)	C(3F)	5291(25)	5736(10)	316(10)	64(7)
O(21)	9963(10)	7510(5)	−2111(5)	17(2)	C(3G)	8838(27)	5581(23)	−542(19)	181(24)

[a] U(eq) is defined as one-third of the trace of the orthogonalized U_{ij} tensor.

Table 3. Principal Bond Lengths [Å] for V_4O_{10}, NC_7H_{14}[a]

Oxide Layers					
V(1)−O(19): 1.56(1)	V(5)−O(25): 1.59(1)	V(9)−O(20): 1.63(1)	V(2)−O(22): 1.57(1)	V(6)−O(24): 1.58(1)	V(10)−O(27): 1.61(1)
V(1)−O(11): 1.79(1)	V(5)−O(17): 1.78(1)	V(9)−O(3): 1.72(1)	V(2)−O(12): 1.75(1)	V(6)−O(16): 1.81(1)	V(10)−O(21): 1.67(1)
V(1)−O(8): 1.80(1)	V(5)−O(5): 1.81(1)	V(9)−O(14): 1.83(1)	V(2)−O(2): 1.87(1)	V(6)−O(15): 1.81(1)	V(10)−O(7): 1.85(1)
V(1)−O(10): 1.86(1)	V(5)−O(13): 1.87(1)	V(9)−O(6): 1.87(2)	V(2)−O(8): 1.96(1)	V(6)−O(13): 1.89(1)	V(10)−O(4): 1.88 (1)
V(1)−O(9): 2.28(2)	V(5)−O(6): 2.13(2)	V(9)−O(5): 2.15(1)	V(2)−O(7): 1.97(1)	V(6)−O(1): 2.15(1)	V(10)−O(12): 2.42(2)
s4 = 4.85	*s4 = 4.82*	*s4 = 4.75*	*s4 = 4.90*	*s4 = 4.71*	*s4 = 4.75*
s5 = 5.10	*s5 = 5.06*	*s5 = 5.00*	*s5 = 5.15*	*s5 = 4.97*	*s5 = 4.91*
V(3)−O(18): 1.58(1)	V(7)−O(30): 1.60(1)	V(11)−O(26): 1.60(1)	V(4)−O(23): 1.60(1)	V(8)−O(29): 1.61(1)	V(12)−O(28): 1.60(1)
V(3)−O(3): 1.88(1)	V(7)−O(11): 1.76(1)	V(11)−O(17): 1.82(1)	V(4)−O(5): 1.88(1)	V(8)−O(2): 1.73(1)	V(12)−O(9): 1.78(1)
V(3)−O(10): 1.89(1)	V(7)−O(6): 1.85(1)	V(11)−O(4): 1.90(1)	V(4)−O(15): 1.90(1)	V(8)−O(1): 1.86(1)	V(12)−O(16): 1.80(1)
V(3)−O(12): 1.92(1)	V(7)−O(1): 1.86(2)	V(11)−O(9): 1.91(1)	V(4)−O(21): 1.96(1)	V(8)−O(14): 1.93(1)	V(12)−O(7): 1.93(1)
V(3)−O(4): 1.96(1)	V(7)−O(13): 2.05(1)	V(11)−O(10): 2.02(1)	V(4)−O(14): 2.00(2)	V(8)−O(15): 2.12(1)	V(12)−O(8): 2.08(1)
s4 = 4.57	*s4 = 4.85*	*s4 = 4.56*	*s4 = 4.32*	*s4 = 4.65*	*s4 = 4.73*
s5 = 4.80	*s5 = 5.10*	*s5 = 4.75*	*s5 = 4.54*	*s5 = 4.89*	*s5 = 4.98*
Quinuclidinium Cations					
N(1)−C(1G): 1.44(2)	N(1)−C(1D): 1.47(3)	N(2)−C(2B): 1.42(2)	N(3)−C(3G): 1.47(3)	N(3)−C(3E): 1.47(3)	N(3)−C(3C): 1.51(2)
N(1)−C(1C): 1.48(2)	N(2)−C(2E): 1.49(2)	N(2)−C(2G): 1.49(2)			
C(1A)−C(1B): 1.46(3)	C(1B)−C(1G): 1.48(3)	C(2A)−C(2D): 1.43(3)	C(2B)−C(2D): 1.52(3)	C(3A)−C(3D): 1.42(4)	C(3B)−C(3E): 1.56(3)
C(1A)−C(1F): 1.53(2)	C(1C)−C(1F): 1.51(2)	C(2A)−C(2F): 1.50(3)	C(2C)−C(2G): 1.59(3)	C(3A)−C(3F): 1.56(3)	C(3C)−C(3F): 1.54(2)
C(1A)−C(1E): 1.55(3)	C(1D)−C(1E): 1.56(3)	C(2A)−C(2C): 1.53(3)	C(2E)−C(2F): 1.52(3)	C(3A)−C(3B): 1.50(3)	C(3D)−C(3G): 1.53(4)
Strongest Hydrogen Bonds					
H(1)−O(25): 2.25(5)	H(1)−O(26): 2.29(5)	H(2)−O(27): 2.24(5)	H(2)−O(23): 2.25(5)	H(3)−O(24): 2.25(5)	H(3)−O(28): 2.33(5)

[a] The sum of the bond valences around each vanadium is also mentioned using the data of ref 12 either considering vanadium as V^{IV} (s4) or V^{V} (s5). The corresponding parameters for the expression $n_{ij} = \exp[(R_{ij} - d_{ij})/b]$ are $R_{ij} = 1.784$ for V^{IV} and 1.803 for V^{V}, b being always 0.37.This paper needs a title running head (TRH).

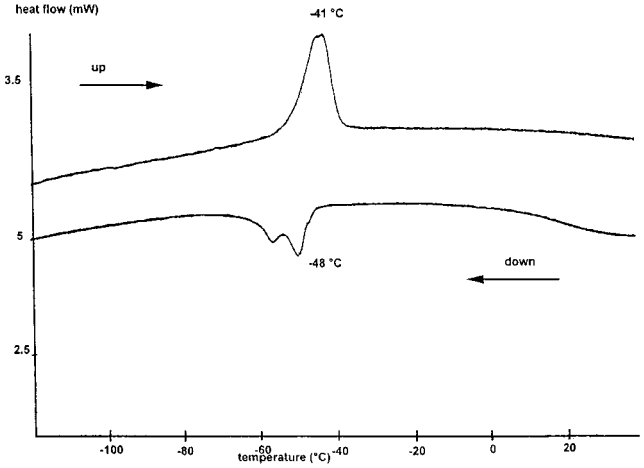

Figure 1. Differential scanning calorimetry curve of V_4O_{10}, NC_7H_{14} powder.

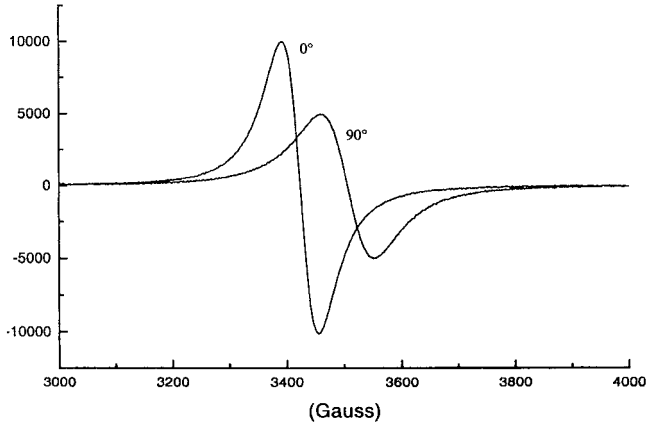

Figure 2. ESR spectra of V_4O_{10}, NC_7H_{14} single crystals recorded at 110 K for $\theta = 0°$ and $\theta = 90°$.

mainly Lorentzian over the entire temperature range. Such a temperature-dependent line broadening should be due to the hopping of unpaired electrons between neighboring V^{4+} and V^{5+} ions. This hopping process is thermally activated and the hopping frequency increases with temperature $\nu = \nu_0 \exp(-E/kT)$. The variation of the line width with temperature on a powder sample is reported in Figure 3. An abrupt change in the $\Delta H = f(T)$ curve is observed between 200 and 230 K, suggesting two different hopping regimes.

Figure 4 reports the temperature dependence of the dc conductivity. The room-temperature electronic conductivity is close to $\sigma = 10^{-4}\ \Omega^{-1}\ cm^{-1}$. It decreases with temperature according to an Arrhenius law. However a discontinuity is observed around 230 K. The activation energy at room-temperature $E_{HT} \approx 0.25$ eV is slightly smaller than the low-temperature activation energy E_{LT}

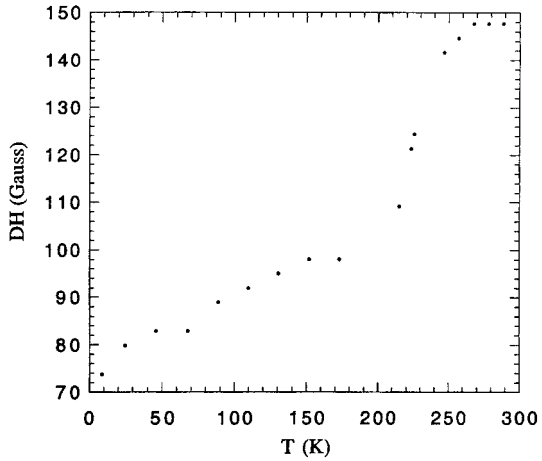

Figure 3. Variation of the ESR line width ΔH as a function of temperature.

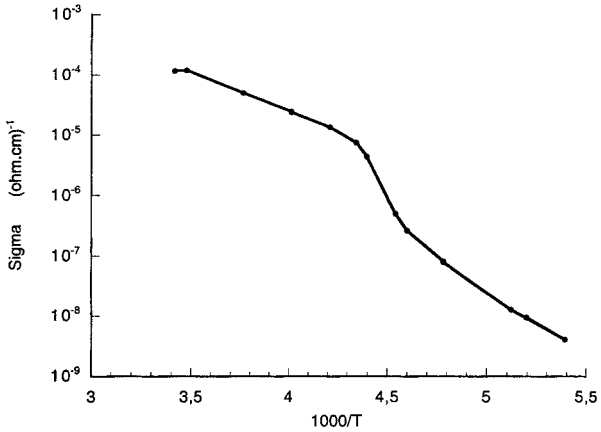

Figure 4. Temperature dependence of the dc conductivity of V_4O_{10}, NC_7H_{14} single crystals along the (010) planes.

≈ 0.35 eV. A transient regime is developed between 210 and 230 K.

Crystal Structure. The cell volume of the low-temperature form (hereafter noted LT) of V_4O_{10}, NC_7H_{14} is three times that of the high temperature form. It means that from the structural point of view, the formula would be $V_{12}O_{30}$, $(NC_7H_{14})_3$. However, for sake of clarity, we shall label the title compound V_4O_{10}, NC_7H_{14} (LT). The metric relationships between the lattice parameters: $a_{LT} = c_{HT}$, $b_{LT} = a_{HT}$, $c_{LT} = 3b_{HT}$ indicate that the modification only concerns the parameter corresponding to the direction of the double ribbons of square pyramids. Indeed, at first glance, the topologies of the HT and LT forms are very similar (Figure 5a−c) with a two-dimensional structure built up from the stacking of mixed-valence vanadium oxide layers between them some organic quinuclidinium cations are inserted (Figure 5). The inorganic slabs correspond to a $[V_4O_{10}]^-$ formulation with a V^{IV}/V^V ratio equal to $^1/_3$. All the vanadium atoms are in square-pyramidal coordination with four long V−O distances in the basal plane and a short V═O linkage in the perpendicular direction (Table 3). The inorganic layers are built up from zigzag double ribbons of edge-sharing square pyramids running along [001] in the low temperature form. In these ribbons, the free terminal apexes of the square pyramids point alternatively on both sides of the slabs with a sequence "two up−two down" (Figure 5a).

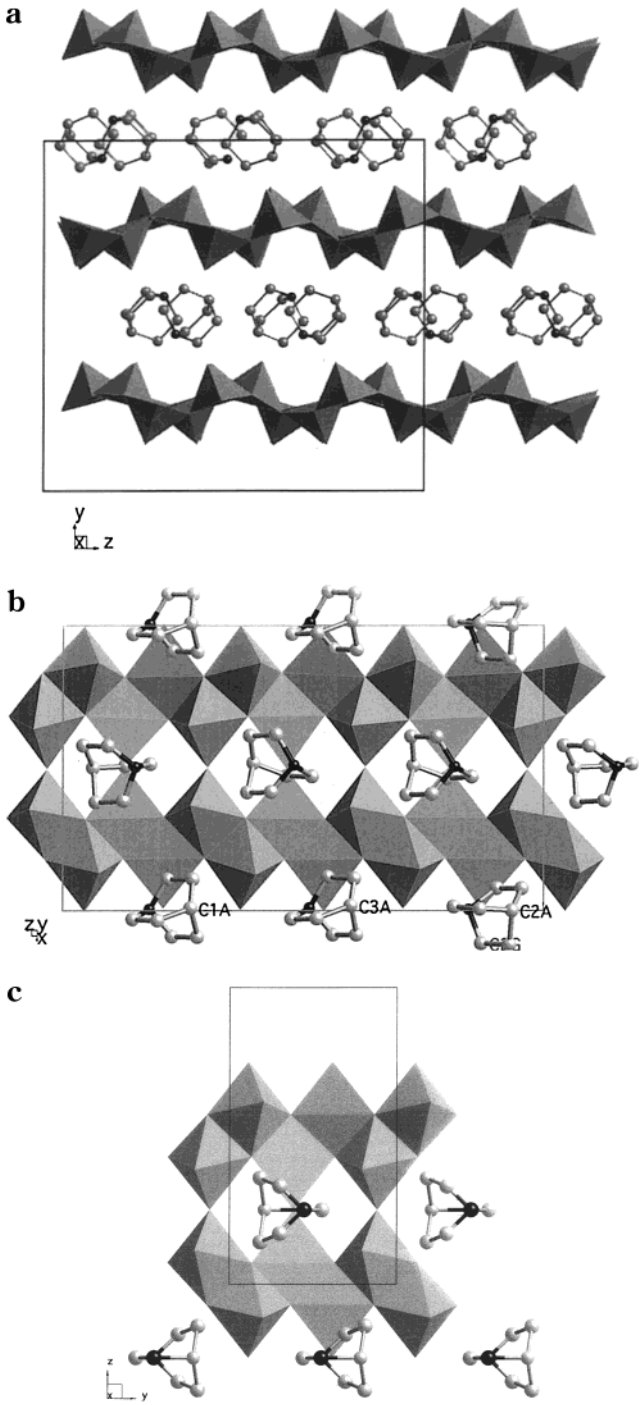

Figure 5. (a) [100] projection of the structure of V_4O_{10}, NC_7H_{14} (LT form) showing the stacking of $[V_4O_{10}]^-$ inorganic layers between which the quinuclidinium cations are inserted; (b) [010] projection of the structure of the LT form; the double ribbons (see text), running along [001] correspond to the sequence "two up-two down" for the orientation of the pyramids; note the particular position of the amine C2A compared to that of amines C1A and C3A, and which is reponsible of the tripling of the c parameter; and (c) [100] projection of the HT form for comparison. Among the two possibilities (see text), the chosen orientation of the amines corresponds to the position directly comparable to those of the LT form.

The double ribbons are linked together by corners which correspond to the remaining oxygen atoms of the basal planes of the square pyramids. The V═O bonds of the two square pyramids involved in the corner linkage are in cis position.

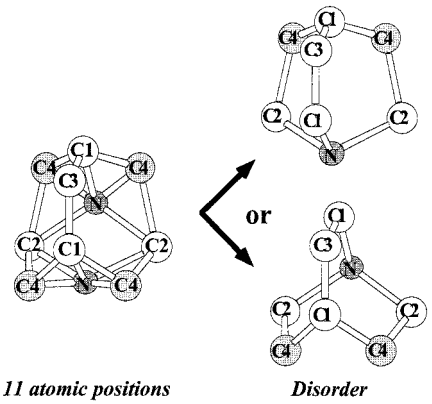

Figure 6. Evidence of the disorder of the quinuclidinium cations in the HT form of V_4O_{10}, NC_7H_{14}.

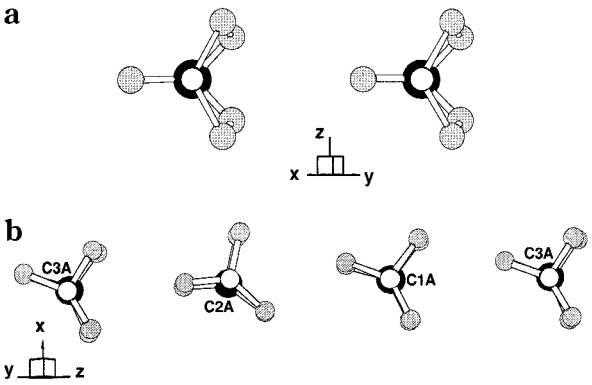

Figure 7. View along the C−N axis of the quinuclidinium ions of the orientation of the amines in (a) the HT form and (b) the LT form. Tertiary carbon, secondary carbon, and nitrogen atoms are represented as black, gray, and white spheres, respectively.

However, some subtle differences exist between the HT and LT forms and a deeper examination of the two structures will first show that the tripling of one lattice parameter is mainly due to the reorientation of some quinuclidinium ions and will further explain the evolution of the electronic properties in relation with the slight modifications induced in the layers by the amine rearrangements.

Indeed, it must be recalled that in the centrosymmetric HT V_4O_{10}, NC_7H_{14}, the quinuclidinium cations were delocalized over two positions each with a 50% probability (Figure 6). This was deduced from the splitting of 11 crystallographic sites into two NC_7 groups of 8 atoms. These two groups can be deduced one from each other by a 100° rotation. In the LT form (Figure 5b), the absence of any disorder on the amine subnetwork gives clear evidence that the transition is related to the reorientation of the latter. For a better comparison between LT and HT forms of V_4O_{10}, NC_7H_{14}, we restricted our analysis to the position of the amine in HT which is the closest to the orientation of quinuclidinium cations in LT and to an examination of the structure in a direction parallel to the C−N axis of the cations. The inclination of the C−N axis toward the $[V_4O_{10}]^-$ layer is almost the same in both structures (51.8° in HT; 50.0 in LT). From Figure 7a,b, it becomes clear that all amines adopt the same orientation in the (001) plane in HT (Figure 7a), whereas in LT, the location of amine 2 (corresponding to C2A label) differs from that of amines 1 and 3 (C1A and C3A labels) by a rotation of 25° around the C−N axis (Figure 7b). Amines 1 and 3 also undergo a rotation of 7° with respect to the situation at room temperature. Therefore, the transition mainly corresponds to (i) an alignment of all the amines of the HT form (50% of them must rotate by 100°), (ii) a slight rotation from the HT values, and (iii) a supplementary rotation of one-third of the amines by 25° which explains the tripling of the *c* parameter of the LT variety.

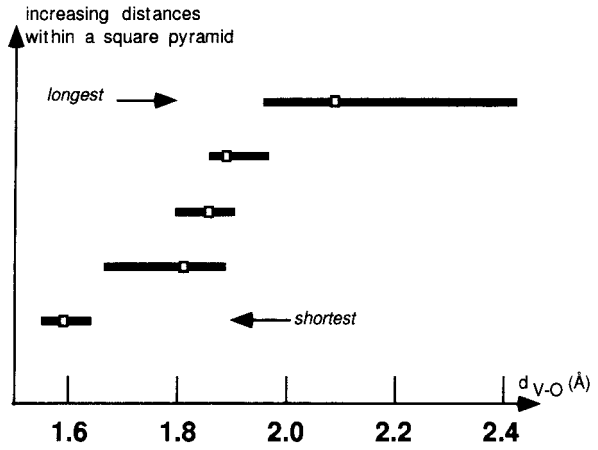

Figure 8. Histogram of the domain of distances observed for each type of V−O bonds in the 12 polyhedra of LT V_4O_{10}, NC_7H_{14}. As all the distances are different in the square pyramids, the *y* axis corresponds to an arbitrary scale in which the shortest distance in the pyramid corresponds to the lower line and the longest to the upper line for each polyhedron. White squares correspond to the distances within the unique vanadium site in the HT form.

Such motions have an influence on the geometric and electronic characteristics of $[V_4O_{10}]^-$ sheets. The first evidence concerns, in the double ribbons, the eclipsed character of two V═O bonds pointing in the same direction within a dimer of edge sharing pyramids. The O═V−V═O angle which is 4.6° in HT and reaches ⟨20°⟩ in LT. Moreover, in the $[V_4O_{10}]^-_{HT}$ layers, vanadium is located on a single crystallographic site. This implies that both V^{IV} and V^V randomly occupy in a $V^{IV}/V^V = {}^1/_3$ ratio the square pyramids, which is in agreement with the observed electron delocalization. Despite a topological similarity, the analysis of the geometrical characteristics of the 12 different square pyramids in the $[V_4O_{10}]^-_{LT}$ layers reveals a rather large distribution of bond distances (Table 3 and Figure 8). It is particularly true for the longest V−O distances (1.96−2.42 Å). That means that the rotation of the amines during the transition has significantly affected the oxygen subnetwork of the layers and the repartition of the distances. It may be thought that the rotation of the amines and the changes in the oxygen subnetwork are cooperative. This last point could indicate a tendency to cationic ordering and therefore a bond-valence analysis using the data of Brese and O'Keeffe[12] was undertaken. It clearly shows that at least V(1), V(2), V(5), V(7), V(9), and V(12) and, for other reasons developed below, V(10) correspond to vanadium(V) since the sum of the bond valences around these vanadium is very close to 5. That means that the other sites contain V^{IV} and V^V, but with a V^{IV}/V^V variable ratios, all larger than ${}^1/_3$, to keep the

(12) Brese, N.; O'Keeffe, M. *Acta Crystallogr.* **1991**, *B47*, 192−197.

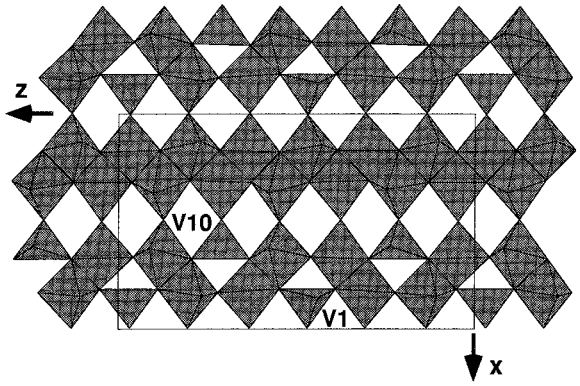

Figure 9. Probable limit structure of LT V_4O_{10}, NC_7H_{14} in which the displacements of oxygens transform the usual 5-fold coordination into tetrahedral one for V(1) and V(10) polyhedra (see text).

global ratio at $^1/_3$. Even if the accuracy of the bond valence analysis is rather poor, it shows the onset of a segregation between V^{IV} and V^V as the temperature decreases below the transition. Moreover, some very long V−O distances [V(1)−O(9) 2.28 Å and V(10)−O(12) 2.42 Å] indicate a lowering of the coordination of these vanadium atoms from a square pyramid to a $4 + 1$ coordination or, more probably, to a tetrahedral one. This is verified by bond valence calculations since the sum of the contributions around O(9) and O(12) is close to 2 (within the usual experimental error) even if V(1) and V(10) contributions are not taken into account. If this is true, Figure 9 would represent the limit structure at low temperature. These structural changes could also provide an explanation for the two different hopping regimes deduced from the ESR measurements of the variation of $\Delta H(T)$, and the existence of two different activation energies observed from the conductivity results.

Finally, two minor structural consequences of the transition must be mentioned: (i) the undulated character of the layer, characterized by the angle between two square planes of adjacent square pyramids, is more pronounced in the LT form (⟨40.4°⟩) than in the HT form (⟨38.2°⟩); (ii) the different orientation of amine 2 in the LT form has a slight incidence on the pyramids surrounding it, with a lowering of the V−O−V angle between two double ribbons (137.4° instead of 145° for amines 1 and 3) and correlatively a decrease of the distance between two apical oxygen of two adjacent square pyramids (3.06 Å instead of 3.29 Å).

Conclusion

These experiments characterized the phase transition of $V^{IV}V^V{}_3O_{10}$, NC_7H_{14} that occurs between 200 and 230 K. From the comparison between the crystal structures of the low and the high temperature forms of V_4O_{10}, NC_7H_{14}, it seems now clear that the transition is due to the ordering of the quinuclidinium cations within the interlayer space. This ordering has consequences on the geometry of the layers which exhibit to some extent the onset of a segregation between V^{IV} and V^V. The latter provides an explanation of the different regimes observed by ESR and conductivity measurements above and below the transition for the electron delocalization which occurs via the overlapping of d_{xy} orbitals along the $[V_4O_{10}]^-$ planes.

Acknowledgment. The authors are very indebted to Dr. A. De Cian (University L. Pasteur, Strasbourg) for its technical help in data collection.

Supporting Information Available: Observed and calculated structure factors for LT-V_4O_{10}, NC_7H_{14}. This material is available free of charge via the Internet at http://pubs.acs.org.

CM9910759